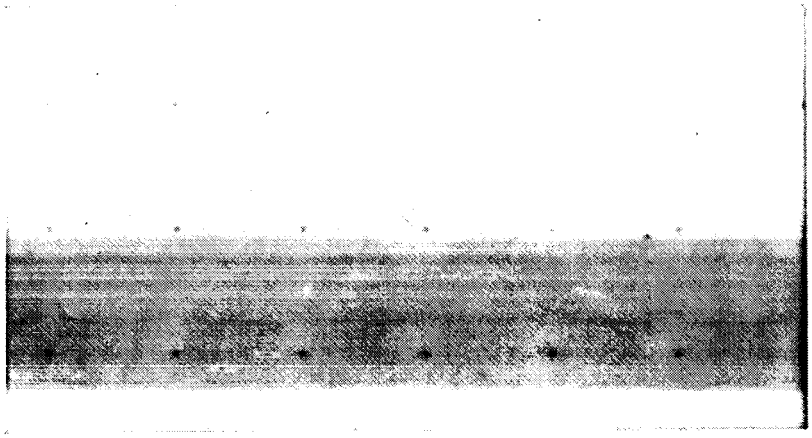

SSL

SPACE SYSTEMS LABORATORY
DEPT. OF AERONAUTICS AND ASTRONAUTICS
MASSACHUSETTS INSTITUTE OF TECHNOLOGY
CAMBRIDGE, MA 02139

EVALUATION OF A SOLAR-BRAYTON SPACE POWER SYSTEM USING THERMAL STORAGE AT REDUCED TEMPERATURE

C.A. Lurio and
M. Martinez-Sanchez

June 1983 SSL#21-83

(Under NASA Grant NAGW-21)

Evaluation of a Solar-Brayton Space Power System using Thermal Storage at Reduced Temperature

by

C.A. Lurio and
M. Martinez-Sanchez

Massachusetts Institute of Technology
Space Systems Lab

June 22, 1983

I. Introduction

Subsequent to the work completed several months ago on solar Brayton/Rankine power systems with thermal energy storage [1,2], some follow-up work was conducted. This was aimed at determining the requirements for a lab scale test of one heat storage/heating tube for the Brayton system.

In the course of this investigation a wider range of sources than originally used were consulted on the question of containability of the postulated molten silicon heat storage material in silicon carbide. The consensus of opinion was that such containment was not possible, that, indeed, the containment of molten silicon for the time required by the power system was unacheivable with any known material. An experiment conducted several years ago at a General Electric research facility had shown that the survival time of silicon carbide holding molten silicon was on the order of days.[3]

With this development we returned to our earlier compilation of heat-of-fusion versus melting temperature to investigate alternative heat storage materials. As a result, MgF_2, with a melting temperature of 1536°K and heat of fusion about half that of silicon, was chosen as the best alternative. Beryllium has a higher heat-of-fusion (at about the same melting temperature) as MgF_2, but was judged to present too many problems of toxicity for the experimentation being considered.

The elimination of silicon as a heat storage material also led to the reevaluation of the basic power system design. It was realized that with the use of the benign He/Xe gas, there was no reason to limit the peak gas temperature during solar influx to that of the MgF_2 storage material - or even that of the silicon if it had been containable. With the use of

carbon/carbon composites for the turbines, peak temperatures to 1900°K and above should be useable.

It was decided to evaluate the possibility of a two-temperature power system. During shadow periods, the peak gas temperature would be limited by the melting temperature of the heat storage material. When out of shadow, the solar influx would directly heat the gas in an extra length of tubing beyond that containing the heat storage substance. One could design this system with a constant generator power output through each orbit or with a lowered output during shadow. In the latter case the deficit between sun and shadow outputs could be partially or fully made up by using batteries.

II. Theoretical Formulation

Thermodynamic

The thermodynamic analysis is identical for both the solar-influx and shadow periods. For the Brayton cycle with regeneration depicted in figure 1 we have the relations

$$\tau_t = 1 - \eta_t + \left[1 - \left(\frac{1}{\pi_c \pi_s}\right)^{\frac{\gamma-1}{\gamma}}\right] \tag{1}$$

$$\tau_c = 1 + \frac{\pi_c^{\frac{\gamma-1}{\gamma}} - 1}{\eta_c} \tag{2}$$

where τ_t and τ_c are turbine and compressor temperature ratios respectively and η_t and η_c are efficiencies for the same. The quantity π_c is the compressor pressure ratio while π_s is a factor representing pressure losses between equipment components of the system.

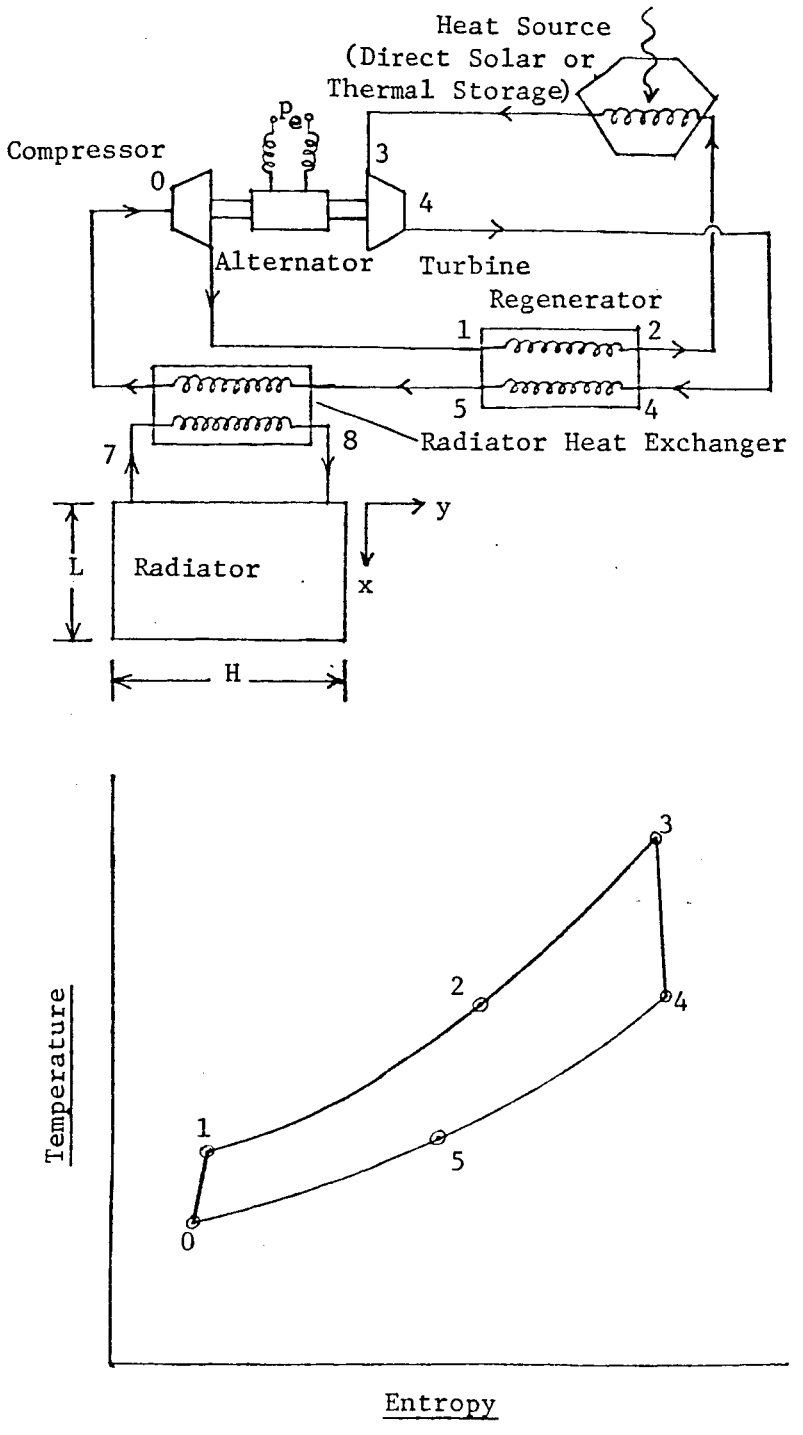

Figure 1: Brayton Cycle with Regeneration

Following the notation of figure 1, we may state

$$T_4 = T_3 \tau_t \tag{3}$$

$$T_0 = \frac{T_7 + (\frac{1}{\varepsilon_2} - 1)(1 - \varepsilon_1)T_4}{\frac{1}{\varepsilon_2} - (\frac{1}{\varepsilon_2} - 1)\varepsilon_1 \tau_2} \tag{4}$$

where ε_1 and ε_2 are the effectivenesses of the regenerator and of the radiator heat exchanger respectively. The latter expression depends upon the assumption that

$$\dot{m} c_p = \dot{m}_R c_{p_R} \tag{4a}$$

where the left side quantities refer to the working gas and those on the right refer to the radiator fluid.

The remaining temperatures and the thermodynamic efficiency in the system (assuming that T_3 and T_7 are specified) can be expressed as

$$T_1 = \tau_c T_0 \tag{5}$$

$$T_2 = T_1 + \varepsilon_1 (T_4 - T_1) \tag{6}$$

$$T_5 = T_4 - \varepsilon_1 (T_4 - T_1) \tag{7}$$

$$T_8 = T_7 + T_5 - T_0 \tag{8}$$

$$\eta_{th} = \frac{(T_3 - T_4) - (T_1 - T_0)}{T_3 - T_2} \tag{9}$$

Radiator

We may equate the electrical power produced by the alternator during the shadow portion of the orbit to that which is demanded from this source by the user (P_{Br}). This gives the quantity

$$\frac{\dot{m}^{sh} c_P}{P_{Br}} = \frac{1}{\eta_a \, \eta_{th}^{sh} \, (T_3 - T_2)^{sh}} \tag{10}$$

where $\dot{m}^{sh}$ is gas flow rate during shadow period, η_a is alternator efficiency (assumed to be identical in sun and shadow) and η_{th}^{sh} is thermodynamic system efficiency in shadow. During the sun period, we may produce a similar formulation but with a required additional term, giving

$$\frac{\dot{m}^{s} c_P}{P_e} = \left[1 + \left(\frac{P_e^{sh}}{P_e} - \frac{P_{Br}}{P_e}\right)\left(\frac{t_{sh}}{t_s}\right) \frac{1}{\eta_B}\right] \frac{1}{\eta_a \, \eta_{th}^{s} (T_3 - T_2)^{s}} \tag{11}$$

where:

$\dot{m}^{s}$ = gas flow rate during solar influx period

P_e = electrical output to user during solar flux

P_e^{sh} = electrical output to user during shadow

t_{sh} = length of shadow period

t_s = length of sun period

η_B = battery efficiency

η_{th}^{s} = cycle thermodynamic efficiency during solar flux.

The additional term in (11) arises from extra power that must be produced during the sun period to charge batteries.

Consider the radiator with dimensions indicated in figure 1. With a manifold such that the coolant is distributed evenly along the length of

the radiator, we can equate net power released to space per unit area at a station y to the power given up by the radiator fluid at that station, i.e.

$$2\varepsilon\sigma(T^4 - T_{BG}{}^4) = \frac{\dot{m}_R}{L} c_{p_R} \frac{dT}{dy} \tag{12}$$

In (12), ε is the radiator emmissivity, σ the Stefan-Boltzmann constant and T_{BG} an effective averaged background temperature. Rearranging (12) and integrating with respect to y results in

$$\frac{\dot{m}_R c_{p_R}}{L} \int_{T_7}^{T_8} \frac{dT}{T^4 - T_{BG}^4} = 2\varepsilon\sigma H.$$

Normalizing T with respect to T_{BG} gives

$$\int_{T_7/T_{BG}}^{T_8/T_{BG}} \frac{dz}{z^4 - 1} = \frac{2\varepsilon\sigma T_{BG}}{\dot{m}_R c_{p_R}} A_R \tag{13}$$

where $z = T/T_{BG}$ and A_R is the radiator area. Integration of the left side of (13) results in

$$A_R = \frac{\dot{m}_R c_{p_R}}{2\varepsilon\sigma T_{BG}^3} \left(-\frac{1}{4} \ln \frac{z+1}{z-1} - \frac{1}{2} \tan^{-1} z\right) \Bigg|_{T_7/T_{BG}}^{T_8/T_{BG}} \tag{14}$$

Dividing both sides by cycle power to the user and using (4a) we have

$$\frac{A_R}{P} = \frac{1}{2\varepsilon\sigma T_{BG}} \left(\frac{\dot{m}c_p}{P}\right) \left[\psi\left(\frac{T_8}{T_{BG}}\right) - \psi\left(\frac{T_7}{T_{BG}}\right)\right] \tag{15}$$

where the definition of ψ follows by comparison with (14). For the sun and shadow periods respectively, then, (15) becomes

$$\frac{A_R^s}{P_e} = \frac{1}{2\varepsilon\sigma T_{BG}^3} \left(\frac{\dot{m}^s c_p}{P_e}\right) \left[\psi\left(\frac{T_8}{T_{BG}}\right)^s - \psi\left(\frac{T_7}{T_{BG}}\right)^s\right] \tag{16a}$$

$$\frac{A_R^{sh}}{P_{Br}} = \frac{1}{2\varepsilon\sigma T_{BG}^3} \left(\frac{\dot{m}^{sh} c_p}{P_{Br}}\right) \left[\psi\left(\frac{T_8}{T_{BG}}\right)^{sh} - \psi\left(\frac{T_7}{T_{BG}}\right)^{sh}\right] \tag{16b}$$

Component masses

The masses of the system components have been found per unit electrical power to the user during the sun period.

To find collector mass, we start with a non-dimensionalized expression for the solar thermal power input requirement,

$$\frac{P_{th}^s}{P_e} = \frac{1}{\eta_{coll}\eta_{th}^s\eta_a} + \frac{1}{\eta_{coll}\eta_{st}\eta_{th}^{sh}\eta_a} \left(\frac{t_{sh}}{t_s}\right)\left(\frac{P_{Br}}{P_e}\right)$$

$$+ \frac{1}{\eta_{coll}\eta_{th}^s\eta_a\eta_B} \left(\frac{t_{sh}}{t_s}\right)\left(\frac{P_e^{sh}}{P_e} - \frac{P_{Br}}{P_e}\right) \tag{17}$$

where for clarity common factors have not been collected. The first term on the right in (17) is that thermal power arising from the electrical requirements of the user during the solar flux period. The quantity η_{coll} refers to the collector efficiency, which accounts for losses from the receiver opening as well as for those due to geometric and surface reflectivity flaws in the mirror. The second term in (17) refers to thermal input required for the thermal energy storage system. The storage system

efficiency η_{st} accounts for losses due to conduction out of and radiation from the receiver. Finally, the last term is the extra thermal power needed to charge batteries (if any) for use during the shadow period.

The mass of the solar collector (assuming an approximately flat surface) is then given by

$$\frac{M_{coll}}{P_e} = \mu_{coll} \frac{1}{S} \frac{P^s_{th}}{P_e} \tag{18}$$

where μ_{coll} is the collector mass per unit area, and S is the solar flux. Thermal storage material and receiver mass are expressed as

$$\frac{M_{st}}{P_e} = (1 + F_{st}) \frac{1}{h_{sf}} \frac{t_{sh}}{\eta_{st}\eta^{sh}_{th}\eta_a} \left(\frac{P_{Br}}{P_e}\right) \tag{19}$$

where h_{sf} is the storage material heat of fusion and F_{st} is a factor to account for the receiver. Battery mass is given by

$$\frac{M_{batt}}{P_e} = \alpha_B \frac{t_{sh}}{\eta_B} \left(\frac{P^{sh}_e}{P_e} - \frac{P_{Br}}{P_e}\right) \tag{20}$$

with α_B being the battery specific mass (kg/joule). For the regenerator we have the expression

$$\frac{M_{reg}}{P_e} = \alpha_{reg} \frac{\dot{m}c_p}{P_e} (T_2 - T_1). \tag{21}$$

Note that the mass is proportional to the temperature rise of the gas from the compressor. The quantities $\dot{m}$ and $(T_2 - T_1)$ are for the sun or shadow period, depending upon which set produces the larger regenerator

mass. The quantity α_{reg} is a mass parameter in kg/watt. Radiator mass, for either the sun or shadow periods is given by

$$\frac{M_{rad}}{P_e} = \mu_{rad} \frac{A_R}{P_e} \tag{22}$$

with μ_{rad} the mass per unit area. Finally, we set a fixed value for the rotating equipment mass of

$$\frac{M_{rot}}{P_e} = 1.5 \text{ kg/kW}_e \tag{23}$$

based upon our past work.[1,2]

Overall efficiency

To provide a basis for comparison of the two-temperature system with conventional devices, we define an averaged system efficiency as

$$\bar{\eta}_c = \frac{t_s P_e + t_{sh} P_e^{sh}}{t_s P_{th}^{s}} \tag{24}$$

III. System Evaluation

Introduction

To minimize system cost and complexity, we treat the power system during shadow as an off design version of that operating during solar flux. This leads to two important problems: matching radiator area requirements during sun and shadow and determining the off-design performance of the turbine/compressor during the shadow period.

Radiator

As shown in equations (16a, b) we may generate separately radiator area requirements for the sun and shadow periods. The most useful way of considering the problem of matching these areas is graphically. Figure 2 shows a series of curves depicting shadow period specific area A_R^{sh}/P_{Br} as a function of radiator fluid exit temperature with turbine pressure ratio as the parameter. Also indicated at several points along the curves are shadow period thermal efficiencies (η_{th}^{sh}'s).

Suppose that we have arrived at a sun period radiator specific area A_R^s/P_e (This having resulted from an optimization of system mass with respect to sun period parameters and with an initial guess of .3 for η_{th}^{sh}.) Using a specified value for P_e/P_{Br} we can plot the area as a straight line running across figure 2. Intersections with the curves represent shadow period operating conditions for which sun and shadow radiator areas are equated. The particular condition the system will run at in the shadow is to be selected from among these intersections by the operating characteristics of the turbomachinery.

Turbine/Compressor

Once a match has been made of radiator areas, we turn our attention to the turbomachinery. For the present we assume that the turbine operates at choked flow conditions during both sun and shadow and consider off-design operation for the compressor only. We assume the use of centrifugal compressors and turbines.

Figure 3 shows the performance map for a typical compressor of this type operating in air. (It is realized that the curve shape will differ

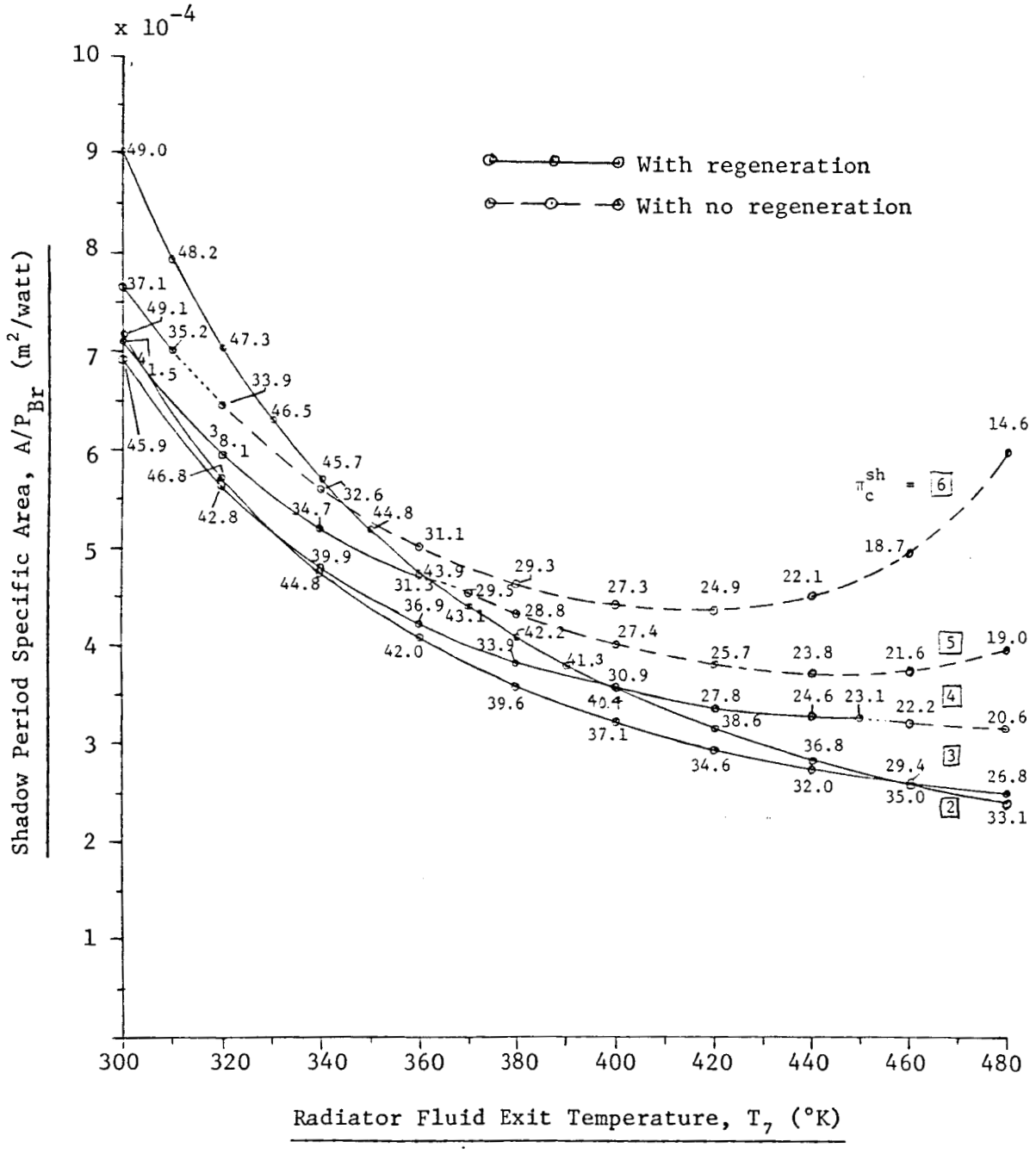

Figure 2: Shadow Period Specific Area versus Radiator Fluid Exit Temperature with Shadow Compressor Ratio (π_c^{sh}) as Parameter

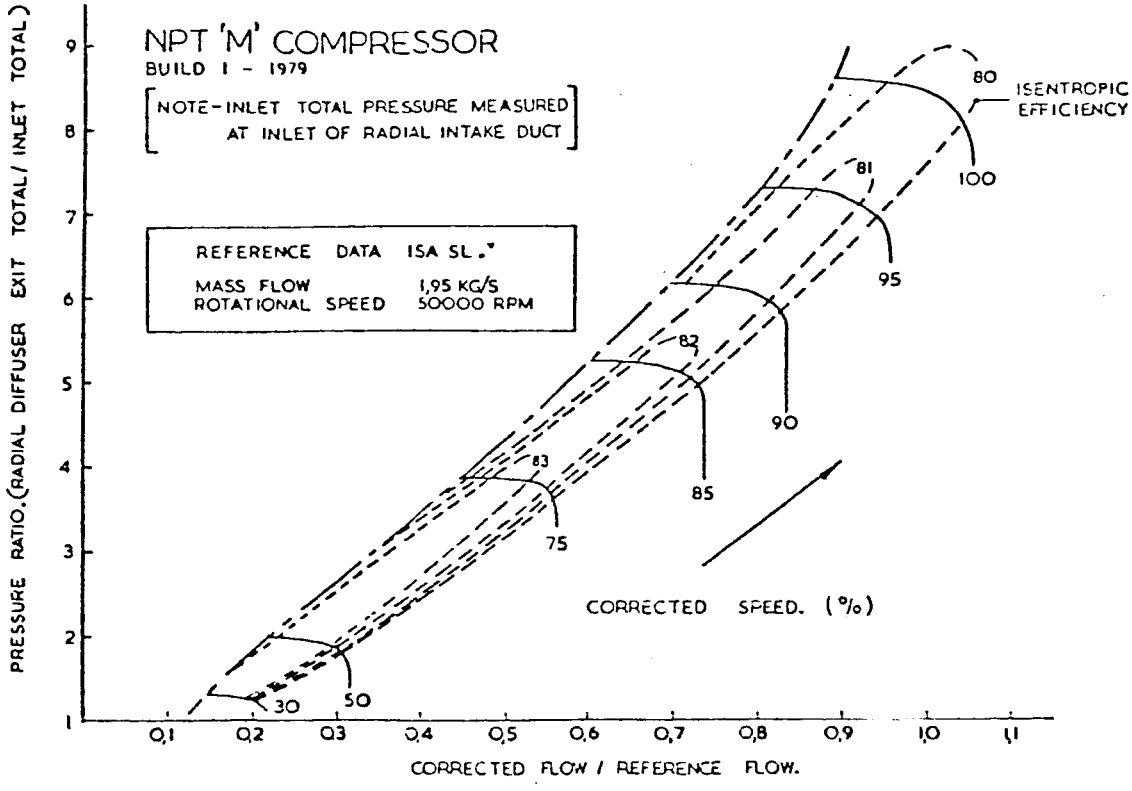

Figure 3: Example of Compressor Performance Map [4]

somewhat for a noble gas, but the main trends and relative positions of important points are expected to be similar.) To use this, we would draw a line across the diagram at the nominal (sun period) compressor ratio. The intersection of this line with the locus of maximum compressor efficiencies would then determine the corrected speed and (corrected flow)/(reference flow) for the compressor at its design condition.

We make the a priori assumption of an 85% compressor design point efficiency. With scaling of the map in figure 3 in the proportion of assumed to map-given nominal efficiency, we can get an idea of what happens at an off-design (shadow operations) point.

We start with the specification that alternator speed must remain at the same level during sun and shadow periods in order to prevent problems with AC loads. For each of the intersection points on the radiator area graph described above, two corresponding points may be plotted in figure 3. One of these points is for corrected speed, the other for corrected flow. Where the lines for these quantities intersect determines the off-design operating point of the compressor.

The definitions of corrected speed and corrected flow (using the notation of figure 1) are given respectively by

$$\text{corrected speed} = \frac{\omega}{\sqrt{T_0}} \tag{25a}$$

$$\text{corrected flow} = \frac{\dot{m}\sqrt{T_0}}{P_0} \tag{25b}$$

where ω is the rotation rate. With the constant ω condition we obtain for a radiation area intersection point,

$$(\text{corrected speed})_{\substack{\text{off}\\\text{design}}} = (\text{corr. speed})_{\text{design}} \sqrt{\frac{(T_0)_{\text{design}}}{(T_0)_{\substack{\text{off}\\\text{design}}}}} \tag{26}$$

Similarly for corrected flow (actually (corrected flow)/(reference flow) for the compressor), we obtain the off-design expression.

$$(\text{corrected flow})_{\substack{\text{off}\\\text{design}}} = (\text{corr. flow})_{\text{design}} \frac{\dot{m}_{\text{off design}}}{\dot{m}_{\text{design}}} \cdot \sqrt{\frac{(T_0)_{\text{off-des.}}}{(T_0)_{\text{design}}}} \cdot \frac{(P_0)_{\text{design}}}{(P_0)_{\substack{\text{off}\\\text{design}}}} \tag{27}$$

The choked turbine assumption can be stated for fixed geometry as

$$\left(\frac{m\sqrt{T_3}}{P_3}\right)_{\text{design}} = \left(\frac{m\sqrt{T_3}}{P_3}\right)_{\substack{\text{off}\\\text{design}}} \tag{28}$$

and we have by definition that

$$\frac{(P_0)_{\text{design}}}{(P_0)_{\substack{\text{off}\\\text{design}}}} = \left(\frac{P_3}{\pi_c}\right)_{\text{design}} \left(\frac{\pi_c}{P_3}\right)_{\text{off design}} \tag{29}$$

combining the last two equations to substitute for $(P_0)_{\text{design}}/(P_0)_{\text{off design}}$ gives

$$(\text{corrected flow})_{\substack{\text{off}\\\text{design}}} = (\text{corr.flow})_{\text{design}} \sqrt{\frac{(T_3)_{\text{design}}}{(T_3)_{\substack{\text{off}\\\text{design}}}}} \cdot \frac{(\pi_c)_{\text{off design}}}{(\pi_c)_{\text{design}}} \sqrt{\frac{(T_0)_{\text{off design}}}{(T_0)_{\text{design}}}} \tag{30}$$

For off-design points that fall substantially out of the area of the compressor map in the figure, we may estimate the compressor efficiency by an approximate form of Euler's equation:

$$\eta_c \simeq \frac{\pi_c^{\frac{\gamma-1}{\gamma}} - 1}{(\text{corrected speed})^2} \tag{31}$$

This must be multiplied by the map scaling ratio cited before to get the estimate for the He/Xe compressor.

Summary of Calculation Procedure

Starting with an assumption of shadow period thermal efficiency of 30%, we match radiator areas using figure 2, whose curves were generated with an assumed $\eta_c^{sh} = .85$. With intersections from figure 2, we plot corrected speed and flow on figure 3. The intersection of these curves, using the estimation and scaling rules discussed above, gives a revised value of η_c^{sh}. The matched radiator areas for this intersection gives a revised value of η_{th}^{sh}. The latter quantity may be used for an estiamte of system mass.

To improve the mass estimate we use the revised η_c^{sh} to generate (implicitly if not explicitly) new values for the curves of figure 2. New radiator area matchings may the nbe made and again we can find the off-design point using figure 3. We now revise the system mass using the value of η_c^{sh} from the first revision. We may repeat the process as long as the compressor graph accuracy permits.

Baselined Parameters

Baselined values for the parameters used are listed in table 1. These are based upon the work of references one and two and the general turbomachinery literature. From a reconsideration of numbers in reference 1, the value of F_{st} was dropped from 1.2 used in reference 2 to 1.0.

Table 1: Baselined Parameters for System Evaluation

$T_3^s = 1900°k$, $T_3^{sh} = 1500°k$, $T_7^s = 350°k$

$\eta_c^s = .85$, $\eta_t = .91$, $\eta_{coll} = .81$, $\eta_{st} = .8$, $\eta_a = .92$, $\eta_B = .75$

$\varepsilon_1 = \varepsilon_2 = .9$

$T_{BG} = 250°k$, $\varepsilon = .75$ $\frac{t_s}{t_{sh}} = \frac{3}{2}$, $s = 1400 W/m^2$

$h_{fg} = 9.4357 \times 10^5 J/kg$ (for MgF_2)

$F_{st} = 1.0$

$\alpha_{batt} = 1.3\overline{88} \times 10^{-5} kg/J$; $\alpha_{reg} = 3.22 kg/kW_t$

$\mu_{coll} = 2.1\ kg/m^2$ $\mu_{rad} = 7.1\ kg/m^2$

Results of Investigation

So far the optimization that has been considered is one with respect to sun time pressure ratio, with no batteries and a constant power output (i.e. $P_e^{sh}/P_e = P_{Br}/P_e = 1$).

Figure 4 shows a comparison of system masses as a function of compressor pressure ratio between first estimates (with $\eta_c^{sh} = .85$) and estimates with revised η_c^{sh}'s. While the revised estimates produce higher system masses, the difference is not large. The lowest mass system still occurs at about $\pi_c^s = 4$. For both the corrected and uncorrected systems, the regenerator mass for shadow operations is larger than that for sun for $\pi_c^s = 3$, 4 and 5. This only means that the real regenerator effectivensss is actually somewhat larger than .9 for the sun period.

Design and off-design points on the compressor map are shown in figure 5 for the $\pi_c^s = 4$ condition. The off-design point was found with a revised, scaled η_c^{sh} of .823. Note that at off-design conditions, the compressor is hugging the high efficiency range. A slightly better revised η_c^{sh} was found for $\pi_c^s = 3$ and a slightly worse one at $\pi_c^s = 5$.

In figure 6 we compare the two-temperature cycle results (with revised η_c^{sh}) to those for a one temperature (1650°k) system using silicon heat storage. We also include the overall cycle efficiency $\bar{\eta}_c$ for each. At low values of pressure ratio, cycle efficiency is high in both systems, due to the large contribution of the regenerator. This carries with it a relatively large regenerator mass. Increasing pressure ratio drops the system mass though the cycle efficiency is going down, because the regenerator is going down in mass.

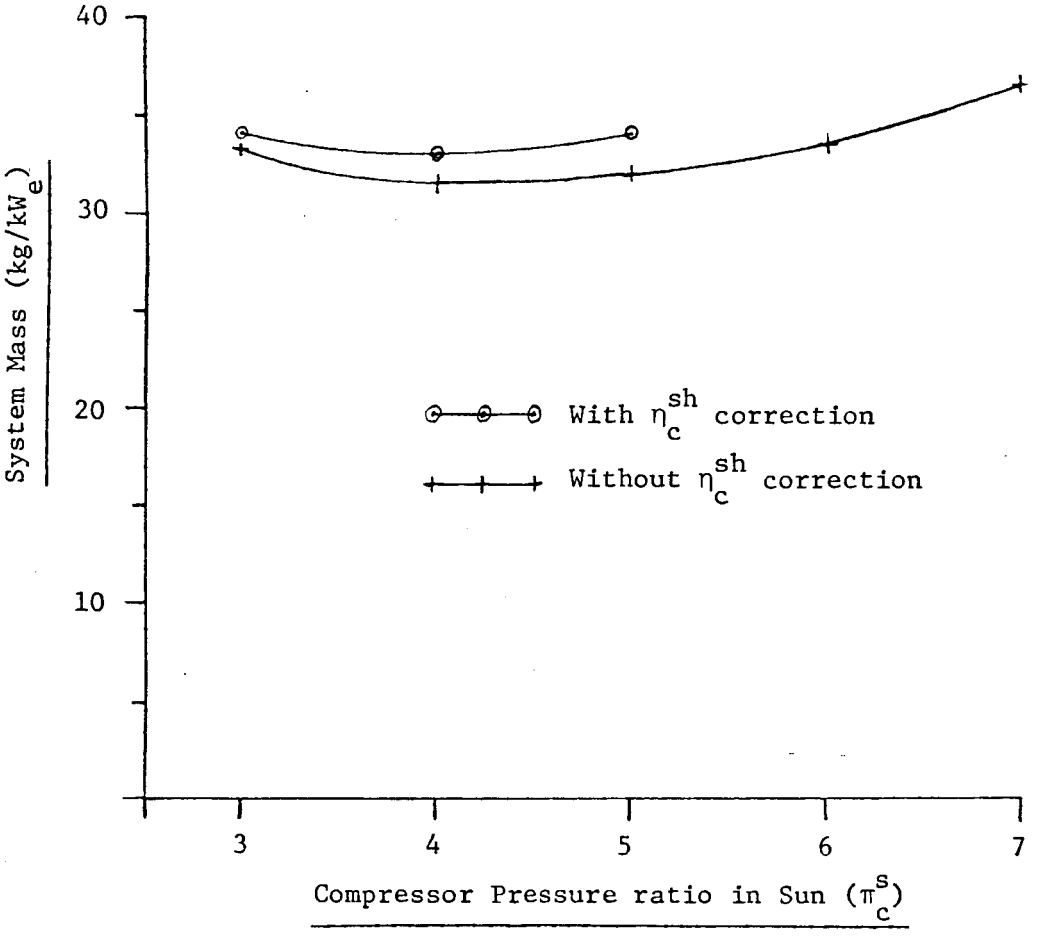

Figure 4: System Mass with MgF_2 Storage vs. Compressor Pressure Ratio in Sun

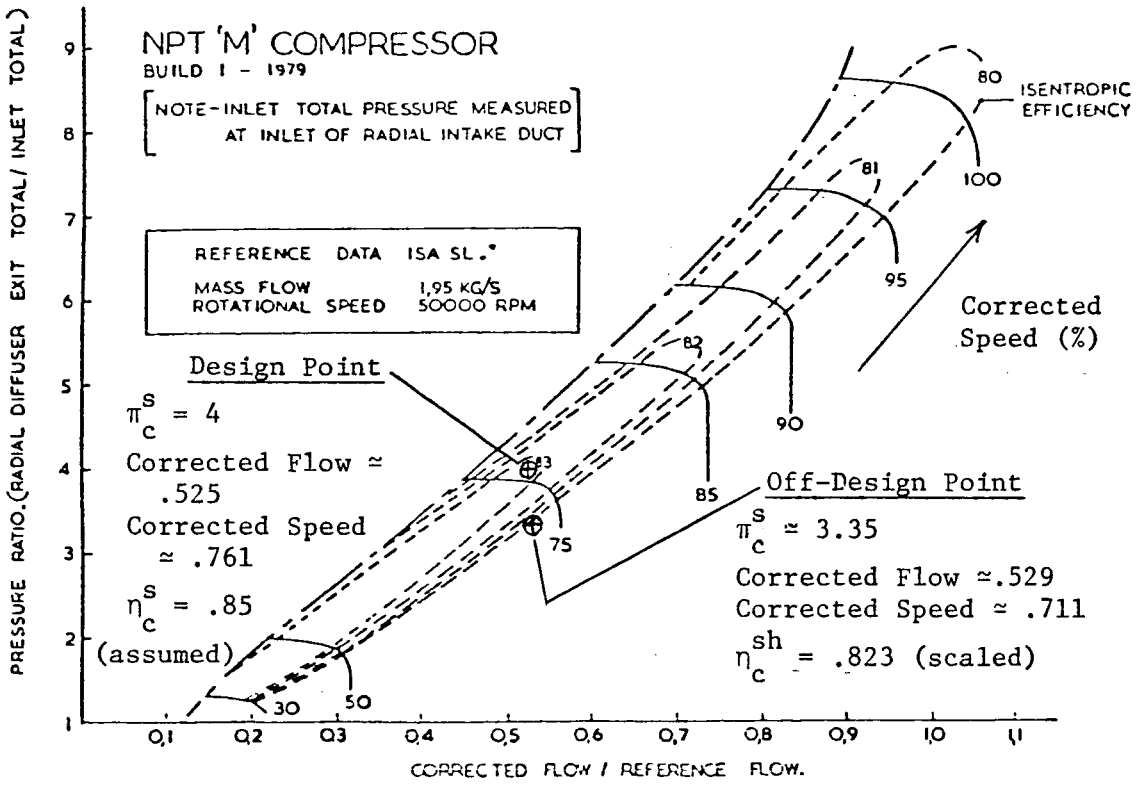

Figure 5: Design and Off-Design (using revised η_c^{sh}) Points for Compressor at $\pi_c^{th} = 4$

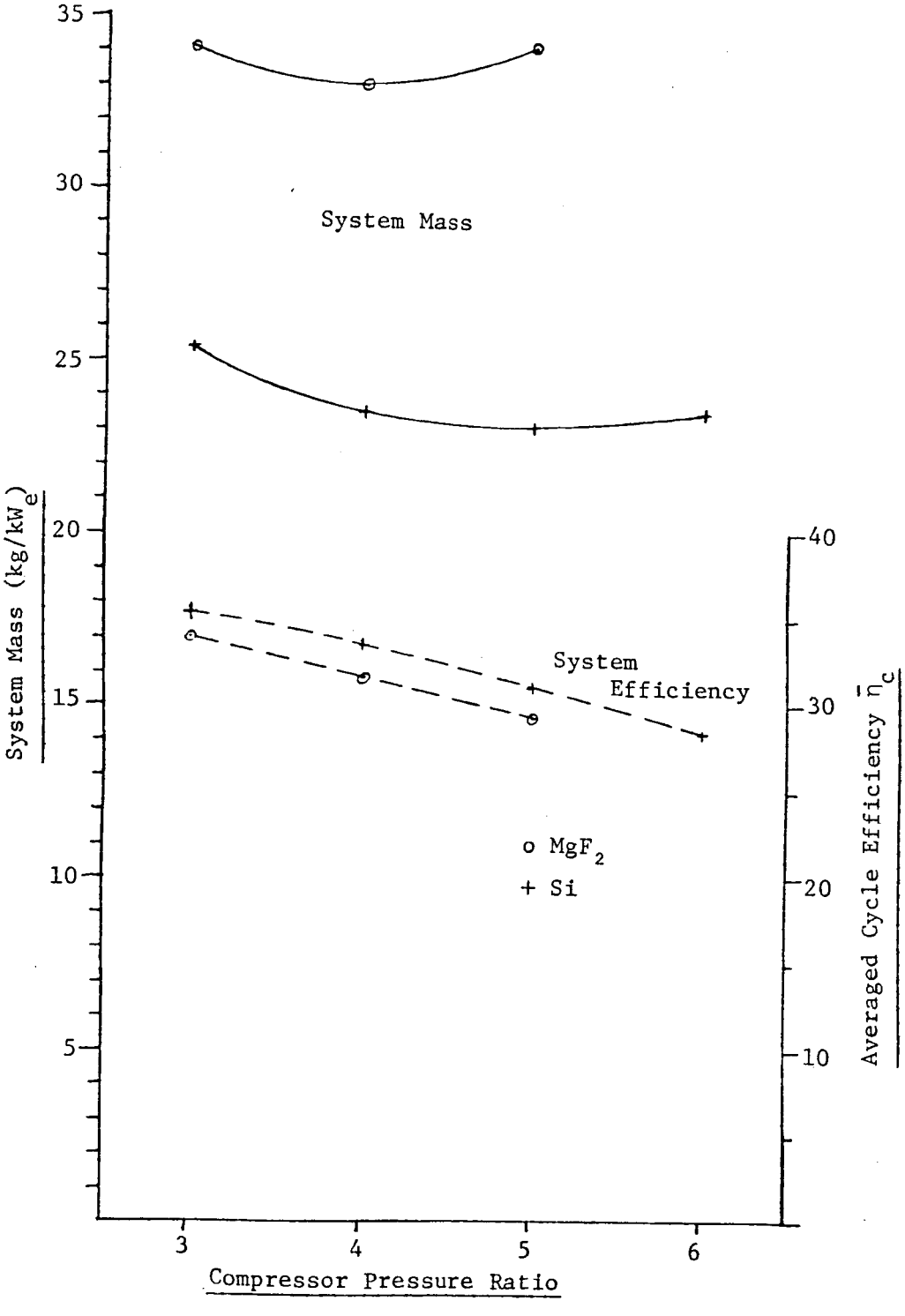

Figure 6: Comparison of Two Storage Types

As pressure ratio continues to increase, the reduction in $\bar{\eta}_c$ causes system mass to again increase. In both systems this is due to an increase in storage and collector requirements as shadow-period efficiency is going down. The pressure ratio in shadow for the two temperature system goes up as π_c^s does.

A comparison of the approximate optima indicated in figure 6 is given in Tables 2a, b. The order of the columns in Table 2a arises from the design sequence: selecting peak temperature, pressure ratio and radiator exit temperature in sun (T_3^s, π_c^s, T_7^s respectively) then attempting to match radiator area in shadow by varying π_c^{sh} and T_7^{sh}.

The bottom radiator temperature in sun is 300°k, which arose from the need to find a sufficient range of π_c^{sh} values for which the radiator areas in sun and shadow can be matched so that an intersection of corrected flow and corrected speed would occur on the compressor map. This low temperature should not pose a problem if a proper mixture of Na and K is used for the radiator fluid (as shown in reference 2) as long as the background temperature is at or above the 250°k average assumed. However, since this <u>is</u> an average, there is a chance of freezing of the radiator fluid, particularly during the shadow portion of the orbit. A way of avoiding this problem would be to use some other fluid in the low temperature part of the radiator.

The shade period radiator bottom temperature is higher than that during the sun. From another point of view we can say that at the off-design point we have a less-efficient system than during sun. That would lead to a larger radiator area unless we drop the sun period bottom radiator temperature to compensate.

Table 2a Thermodynamic Quantities and Specific Radiator Areas at Optimum Sun Period Compressor Pressure Ratios

Storage Type		T_3 (°K)	π_c	T_7 (°K)	$\frac{A}{P_e} \times 10^{-4}$ (m^2/W)	T_0 (°K)	T_1 (°K)	T_2 (°K)	T_4 (°K)	T_5 (°K)	T_8 (°K)	η_{th}	$\bar{\eta}_c$
MgF_2	Sun	1900	4	300	4.540	338.9	634.5	1130	1185	689.5	650.5	.5450	.3155
	Shade	1500	3.35	351.9	4.540	387.9	680.9	962.7	994.1	712.2	676.2	.3964	
Si		1650	5	300	5.826	343.3	708.2	929.1	953.6	732.8	689.5	.4598	.3115

Table 2b Mass Comparison at Optimum Sun Period Compressor Pressure Ratios

Storage Type	$\frac{M_{coll}}{P_e}$ ($\frac{kg}{kw}$)	$\frac{M_{sto}}{P_e}$ ($\frac{kg}{kw}$)	$\frac{M_{reg}}{P_e}$ ($\frac{kg}{kw}$)	$\frac{M_{rad}}{P_e}$ ($\frac{kg}{kw}$)	$\frac{M_{rot}}{P_e}$ ($\frac{kg}{kw}$)	$\frac{M_{total}}{P_e}$ ($\frac{kg}{kw}$)
MgF_2	7.925	15.69	4.632	3.223	1.5	32.97
Si	8.027	7.131	2.332	4.137	1.5	23.13

The main difference between the systems is in heat storage, with about twice the mass required for the MgF_2 system. This mainly arises from the different heats of fusion, with a smaller effect from the different shadow period cycle efficiencies.

At the same time, there is a slightly larger collector mass for the system using Si storage, which may be attributed to the slightly smaller value of $\bar{\eta}_c$.

References

1 Lurio, Charles A., An Evaluation of Solar Mercury Rankine Space Power. Space Systems Laboratory Report #3-83, January 1983.

2 Whittinghill, George R., Preliminary Design of a High Temperature Solar Brayton Space Power System. Space Systems Laboratory Report #7-83, February 1983.

3 Personal communication with Dr. Robert Gidding, General Electric Corporate Research Development Center, Schenectady, NY.

4 Chevis, R.W. and Varley, R.J., "Centrifugal Compressors for Small Aero and Automotive Gas Turbine Engines", AGARD Conference Proceedings No. 282: Centrifugal Compressors, Flow Phenomena and Performance, Technical Editing and Reproduction Ltd., London, November 1980, pp. (21-1) - (21-17).